# CHAPTER 3
# *IN SITU* PHOTOCROSSLINKING OF CINNAMATE FUNCTIONALIZED POLY(METHYL METHACRYLATE-CO-2-HYDROXY ETHYL ACRYLATE) FIBERS DURING ELECTROSPINNING[†]

## 3.1 Chapter Summary

A novel methodology for *in situ* crosslinking of polymeric fibers *during* electrospinning is described. The electrospinning apparatus was modified to facilitate UV irradiation of the electrospun fibers while in flight to the collector target. Three copolymers with different mol% of the photoreactive cinnamate functional group (4, 9 and 13 mol% respectively) were synthesized and utilized for this study. Fibers of cinnamate functionalized poly(methyl methacrylate-co-2-hydroxy ethyl acrylate) were crosslinked *in situ* by UV irradiation during electrospinning. Subsequent FTIR measurements on irradiated and non-irradiated electrospun fibers indicated both [2π+2π] cycloaddition of the vinylene C=C and *trans-cis* photoisomerization of the cinnamate group. Furthermore, the irradiated copolymers were observed to form insoluble gels which indicated that the photodimerization was the primary photoprocess during UV irradiation leading to the formation of a crosslinked network. As expected, it was found that the gel fraction increased with increasing mol% of the cinnamate species.

## 3.2 Introduction

Polymers that are sensitive to ultraviolet (UV) irradiation have been widely utilized as photoresists. For instance, in the manufacture of printed circuit boards,[1] negative photoresists are coated on a conducting substrate. A patterned mask placed over the coated substrate then imprints a conducting circuit when the substrate is washed with a solvent to remove the non-irradiated photoresist. Conventional negative-working photoresists based on poly(vinyl cinnamate) (PVCi) and its derivatives have played a leading role in the scientific development of photopolymers since their invention more than four decades ago.[2] The photofunctionality of PVCi arises from photodimerization that leads to insolubilization due to the formation of crosslinks. In the late 1970s, it was reported[3,4] that the photoinduced chemical transformation of PVCi and its derivatives

[†] P. Gupta, S. R. Trenor, T. E. Long, G. L. Wilkes, *Macromolecules* **2004**, *37*, 9211-9218.

resulted in a novel optical property, i.e., induction of birefringence in thin films of PVCi upon exposure to linearly polarized photoirradiation. The further advancement in polarization photochemistry of ultrathin films leading to regulation of the orientation of liquid crystal (LC) molecules[5-11] resulted in an enhanced interest in PVCi. More specifically, it has been observed that PVCi and its derivatives induce the alignment of LCs in contact with the film surface upon irradiation with linearly polarized ultraviolet light. In addition to these unique properties, the ability of the cinnamate group to undergo rapid photodimerization without the addition of a photoinitiator is critically important in the context of the present investigation, as will become more apparent later.

The photochemistry of cinnamates involves two photoreactions upon irradiation in the ultraviolet-B (UVB) region of the electromagnetic spectrum[12-14]; the *trans-cis* isomerization that is favored in the early stages of UV irradiation[15-17] (Scheme 3.1) and the photodimerization from head to head and head to tail [$2\pi + 2\pi$] cycloaddition leading to the formation of a cyclobutane ring (Scheme 3.2). It is believed that during UV irradiation, photodimerization is the major photoprocess, while the *trans-cis* photoisomerization is the minor photoprocess.[18,19] In the present study, cinnamate functionalized polymers were electrospun and *simultaneously* irradiated in the UVB region to produce crosslinked fibers.

Electrospinning is a unique process to produce submicron polymeric fibers in the average diameter range of 100 nm-5 μm.[20-23] Fibers produced by this approach have a diameter that is at least one or two orders of magnitude smaller than those produced by conventional fiber production methods like melt or solution spinning.[24] Recently, researchers have also employed several post-electrospinning processing techniques to produce electrospun fibers that find utility in novel applications. For instance, electrospun fibers of 2-acrylamido-2-methyl-1-propanesulfonic acid doped polyaniline were coated uniformly with thin films of nickel by an electroless deposition technique[25]. The resulting high surface area metal-coated fibrous polymer substrates displayed high conductivity, thereby combining the dual benefits of electrospinning (to produce high surface area fibers) with electroless metal deposition (to make conducting polymer substrates). In a different study, ultrafine mats of oxidized cellulose were prepared by electrospinning of cellulose acetate followed by its subsequent deacetylation and oxidation. Direct

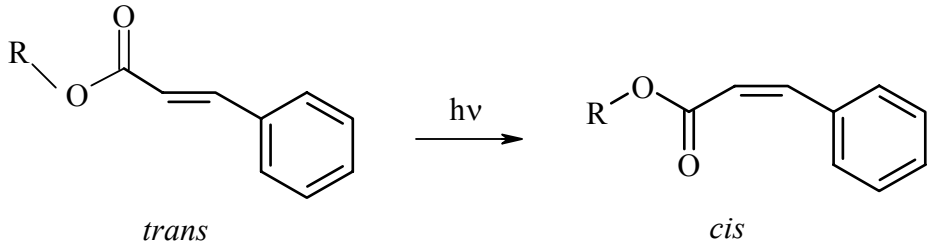


**Scheme 3.1** *Trans-cis* photoisomerization of the cinnamoyl moiety.

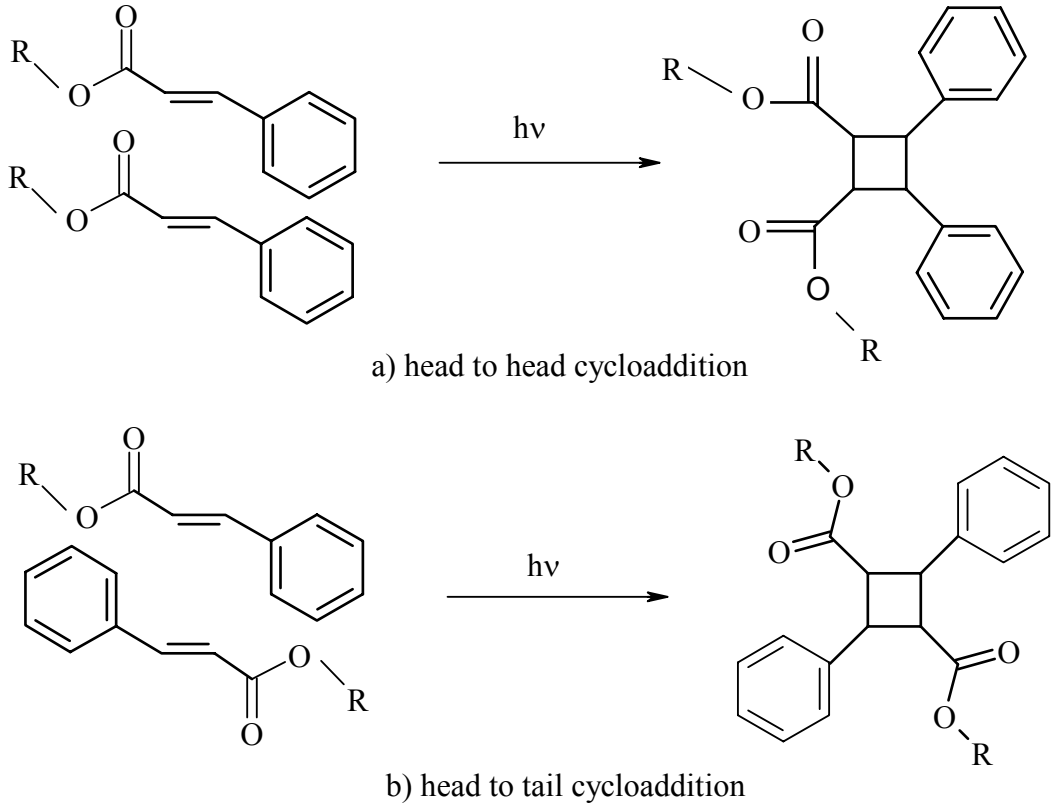


**Scheme 3.2** a) Head to head and b) head to tail photodimerization of the cinnamoyl functional group.

electrospinning of oxidized cellulose is not feasible because of its low solubility in most organic solvents. As a result, post deacetylation and oxidation of electrospun cellulose acetate was performed to produce mats that potentially serve as flexible adhesion barriers and as immobilizing matrices for various drugs, enzymes and proteins.[26] Another post-

electrospinning process that more specifically relates to the present study involved crosslinking of photocurable poly(vinyl alcohol) (PVA) fibers. Electrospun mats of partially esterified PVA containing thienyl acrylate groups were subjected to UV irradiation (λ>300nmn) to produce crosslinked PVA fibers. The UV-irradiated fibers displayed excellent water stability in stark contrast to the PVA fibers produced without UV irradiation.[27] In the experimental approaches that are discussed above, the post-electrospinning processes involved metal-coating, oxidation or crosslinking of the electrospun substrate, which enhanced the fiber properties and lead to new applications. In the following sections, a new method that involves *simultaneous* crosslinking and electrospinning of photocrosslinkable polymers will be discussed. A new device that was designed and fabricated especially to facilitate these two processes to occur in tandem, will be described in detail. Using this novel technique, post-electrospinning operations are eliminated, resulting in a more time-efficient and dynamic process. It should be noted that in addition to the design of the device, the choice of the photocurable functional group is also very important. As mentioned earlier, the cinnamate group undergoes a rapid photodimerization in the UVB region without the addition of any photoinitiators.

In the present study, poly(methyl methacrylate-co-hydroxy ethyl acrylate) [poly(MMA-co-HEA)] was synthesized and subsequently functionalized with cinnamoyl chloride via a quantitative esterification reaction. The cinnamate-functionalized polymers were then irradiated with UV *in situ* during the electrospinning process to form crosslinked fibers in a single processing step. The extent of the photoreactions was monitored with Fourier transform infrared (FTIR) spectroscopy and gel fraction analysis. The morphology of the electrospun mat before and after UV irradiation was investigated using scanning electron microscopy (SEM).

### 3.3 Experimental

#### 3.3.1 Materials

Cinnamoyl chloride, ethyl acetate, and 2,2'-azobisisobutyronitrile (AIBN) and dimethyl formamide (DMF) were purchased from Sigma Aldrich. Methyl methacrylate (MMA) and 2-hydroxyethyl acrylate (HEA), also purchased from Sigma Aldrich, were passed through a neutral alumina column to remove radical inhibitors. Tetrahydrofuran

(THF) was distilled from sodium/ benzophenone under a nitrogen atmosphere prior to polymer/acid chloride reactions.

### 3.3.2 Synthesis and characterization of 85:15 mol% MMA:HEA precursor copolymers

MMA (40.0 g, 465 mmol) and HEA (9.52 g, 81.9 mmol) were added to a 500 mL round-bottomed flask containing a magnetic stir bar. This reaction mixture was diluted with ethyl acetate (205 mL, 80 vol%) followed by the addition of the initiator, AIBN (40.3 mg, 0.1 wt%), to the reaction vessel equipped with a water condenser. The reaction mixture was purged with nitrogen gas for 10 min and maintained at 75 $^{o}$C. Polymerization was allowed to occur for 24 h. The resultant copolymer was precipitated into methanol followed by drying in vacuum at 65 °C for 24 h. $^{1}$H NMR spectroscopy and gel permeation chromatography (GPC) was used to determine the molecular weight and content of HEA incorporated in the copolymer.

$^{1}$H NMR spectra were recorded using a Varian Unity 400 MHz spectrometer at 25 °C in $CDCl_3$. Absolute number and weight average molecular weights of the precursor copolymers were determined at 40 °C in THF (HPLC grade) at 1 mL/min on a Waters 707 Autosampler GPC equipped with 3 in-line PLgel 5 mm MIXED-C columns and an in-line Wyatt Technology Corp. miniDAWN® multiple angle laser light scattering (MALLS) detector.

### 3.3.3 Functionalization of poly(MMA-co-HEA) with cinnamoyl chloride and its characterization

Poly(MMA-co-HEA) (5.00 g) was dissolved in 40 mL of freshly distilled THF. Triethylamine (0.644 g, 6.37 mmol) was added to the reaction mixture followed by stirring under a nitrogen-purge. Cinnamoyl chloride (1.06 g, 6.37 mmol) was dissolved in 5 mL of distilled THF and added drop-by-drop via an addition-funnel to the reaction mixture. This reaction mixture was stirred overnight at 0 °C and stored under a nitrogen-blanket with the reaction vessel covered in aluminum foil to avoid any ambient photoreactions that might be induced by laboratory lighting. Next filtration of the functionalized copolymer was performed followed by its precipitation into approximately 300 mL of 4:1 methanol:water solution. The precipitate was stored in a 60 mL glass bottle that was wrapped with aluminum foil to avoid any exposure from ambient light and

dried under vacuum at 65 °C for 24 h. The isolated yield of the functionalized copolymer was 90%. The reaction is depicted in Scheme 3.3. Three copolymers with different levels of cinnamate functionalization were synthesized for this study and the compositions are provided in Table 3.1.

Differential scanning calorimetry (DSC) analysis of the functionalized copolymers was performed on a Perkin Elmer Pyris 1 DSC at a heating rate of 10 °C/min under a nitrogen purge. The glass transition temperature ($T_g$) was determined from the second heat scan at the midpoint of the glass transition endotherm. The glass transition temperatures of the three functionalized copolymers are also listed in Table 3.1. UV-Vis spectroscopy was performed on a Analytical Instrument Systems Inc. spectrometer that was equipped with fiber optic light guides, a DT1000CE light source, and an Ocean Optics USB2000 UV-Vis detector.

### 3.3.4 *In situ* UV irradiation during electrospinning

The three functionalized copolymers were dissolved separately in DMF at a concentration of 20-wt%. Prior to electrospinning, the viscosities of these solutions were measured with a AR-1000 Rheometer, TA Instruments Inc. The measurement was performed in the continuous ramp mode at room temperature (25 $^{o}$C) using cone and plate geometry. The sample was placed between the fixed Peltier plate and a rotating cone (diameter: 4 cm, vertex angle: 2$^{o}$) attached to the driving motor spindle. The changes in viscosity and shear stress with change in shear rate were measured. A computer interfaced to the equipment recorded the resulting shear stress vs. shear rate data. For the three solutions investigated for the present study, the shear stress vs. shear rate behavior was linear, indicating Newtonian behavior. The slope of the linear shear stress-shear rate relationships (valid in the range of 1-1000 $s^{-1}$ for ST2-126A & B and 0-300 $s^{-1}$ for ST2-127) gave the Newtonian or zero shear rate viscosities, $\eta_o$. These values are reported in Table 3.1. The viscosity of the polymer solutions is an important parameter that influences the final diameter of the electrospun fibers.[28-30] It is important to note, however, that the extensional viscosity of the jet, while in flight to the target is undoubtedly very influential in governing the stretching induced in the jet. However, to the authors' knowledge, a thorough study of the effect of extensional viscosity on fiber formation in electrospinning has not been reported to date. The schematic of the

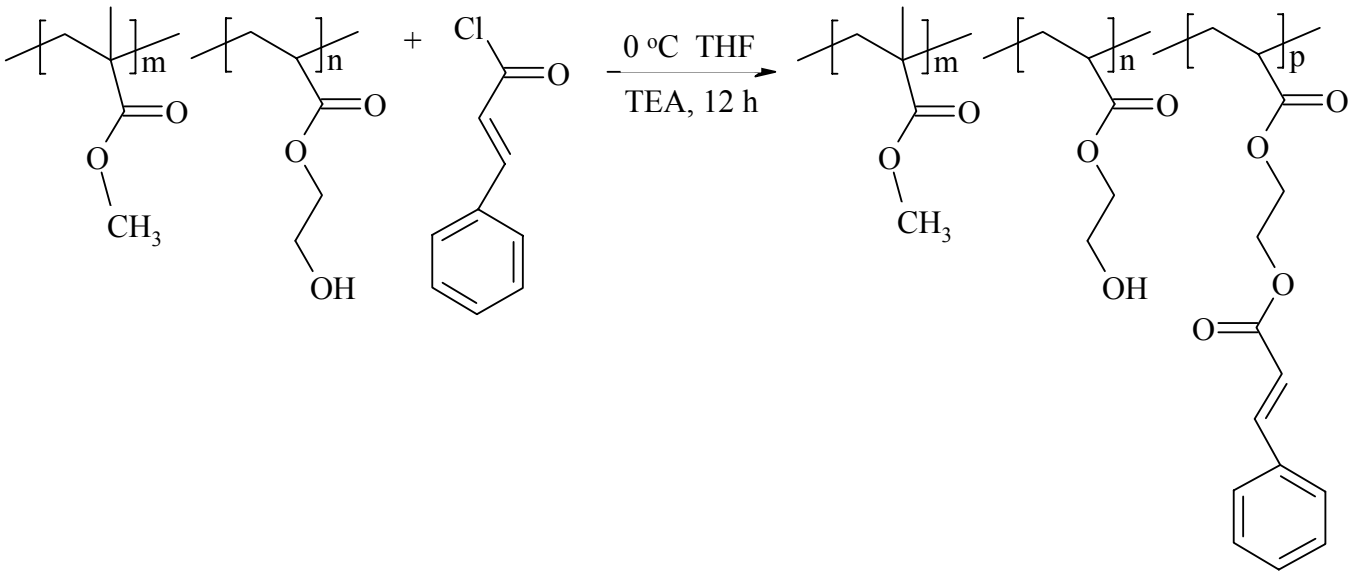


**Scheme 3.3** Functionalization of poly(MMA-co-HEA) with cinnamoyl chloride

**Table 3.1** Chemical composition of the functionalized copolymers and zero shear rate viscosity ($\eta_o$) of their respective 20 wt% solutions in DMF.

| Sample | mol% MMA, (x) | mol% HEA, (y) | mol% cinnamate, (z) | Tg ($^oC$) | $\eta_o$ of a 20 wt% solution in DMF, (Pa.s) |
|---|---|---|---|---|---|
| **ST2-127** | **87** | **9** | **4** | **99** | **2.48** |
| **ST2-126A** | **87** | **4** | **9** | **94** | **0.56** |
| **ST2-126B** | **87** | **0** | **13** | **91** | **0.72** |

electrospinning apparatus with the UV source (F300S Fusion UV Systems, Inc. type 'H' bulb') utilized for irradiation is shown in Figure 3.1. Electrospinning was performed in a vertical configuration where the fibers were electrostatically conveyed in the upward direction to the grounded target. This was done to minimize the heating effects that could arise from exposure to the highly intense UV beam. The apparatus was kept in a fume hood where an airflow was maintained from the bottom to top. The syringe containing the functionalized polymer solution was connected to a Teflon needle (0.7 mm internal diameter). The free-end of the Teflon needle was placed at the entrance of a 15 cm long quartz tube (15 cm internal diameter). A grounded steel wire mesh that served as the

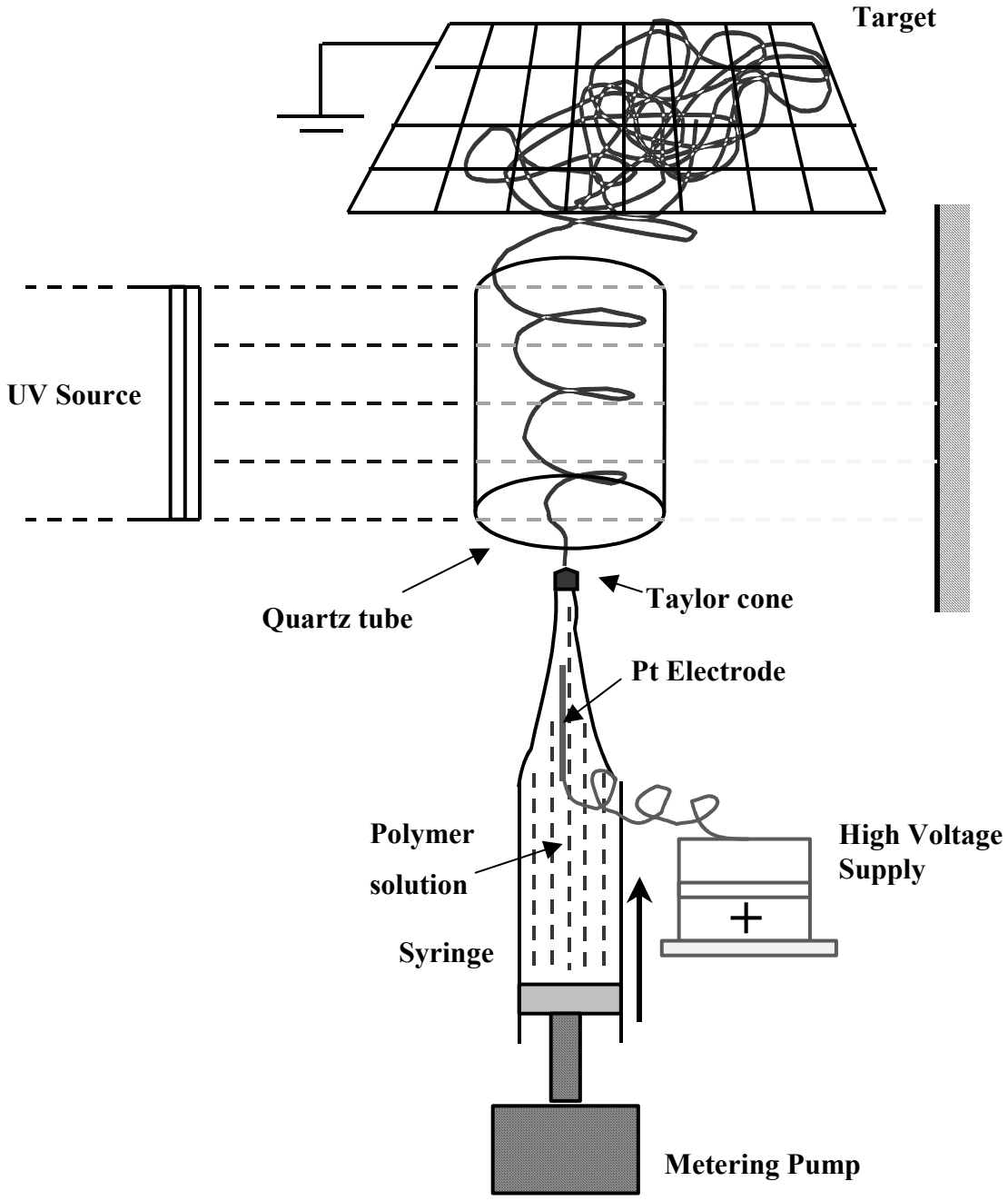


**Figure 3.1** Schematic of the apparatus depicting the UV irradiation of electrospun fibers.

target was placed 5 cm away from the other end of the quartz tube, and the total distance between the Teflon needle tip and target was 20 cm. A platinum electrode dipped in the

morphology of the electrospun mat. A Cressington® 208HR sputter-coater was utilized to sputter-coat the electrospun fiber samples with a 5 nm Pt/Au layer to minimize the polymer solution was connected to a high voltage DC supply with positive polarity. A syringe pump connected to the syringe controlled the flow rate emanating out of the Teflon needle tip.

For each of the three solutions, electrospinning was performed at 15kV, 3 mL/h, 20 cm at a concentration of 20 wt% in DMF. At the tip of the needle, the solution was observed to elongate into a conical shape, also referred to as the Taylor cone.[31] A jet was observed to emanate from the apex of the Taylor cone that traveled through the quartz tube to the grounded target. *During its travel through the quartz tube*, the jet was exposed to the intense UV beam (UVB intensity of 0.135 W/cm$^2$) to allow for irradiation of the cinnamate groups. The quartz tube concentrates/partially focuses the UV beam on the spiraling and looping jet. Samples collected for 10 min with and without UV irradiation were dried in vacuum at 40 $^o$C for 8h. A Leo® 1550 Field Emission Scanning Electron Microscope (FESEM) was utilized to visualize the electron charging effects. In addition, absorbance of the electrospun mats with and without UV irradiation was measured (in transmission mode) in the infrared region (4000 – 400 cm$^{-1}$) on a Nicolet 510 FTIR Spectrometer. Gel fraction analysis of electrospun mats (with and without UV irradiation) was also conducted via a soxhlet extraction process in refluxing THF for 4 h.

### 3.4 Results and Discussion

#### 3.4.1 Synthesis and Modification of Poly(MMA-co-HEA)

The precursor poly(MMA-co-HEA) copolymer was synthesized via an AIBN initiated conventional free radical solution polymerization in ethyl acetate. The resulting copolymer exhibited an absloute weight average molecular weight of 333,000 g/mol with a polydispersity of 1.96. The composition of the copolymer was examined using $^1$H NMR spectroscopy. The results corresponded well with the feed ratios of 87 mol% MMA and 13 mol% HEA.

Modification of poly(MMA-co-HEA) with cinnamoyl chloride was conducted via an esterification reaction between the hydroxyl group of the HEA and cinnamoyl chloride (Scheme 3.3). Adjustment of the molar ratio of cinnamoyl chloride to the hydroxyl functionality was utilized to control the level of functionalization. Three functionalized

MMA-co-HEA copolymers were synthesized with cinnamate concentrations of 4.0, 9.0 and 13 mol% respectively (Table 3.1) utilizing the same precursor unfunctionalized copolymer mentioned previously. $^{1}$H NMR spectroscopic analysis of the cinnamate functionalized poly(MMA-co-HEA) confirmed functionalization of the copolymers at three different levels of the cinnamate functionality. The resonances associated with the cinnamate group were apparent at 7.73, 7.52, 7.38, and 6.49 ppm. A reduction in the peak area of the methylene adjacent to the hydroxyl at 3.75 ppm was observed in addition to the corresponding appearance of the methylene resonance adjacent to an ester linkage at approximately 4.42 ppm. A typical UV absorbance spectra of a cinnamate functionalized poly(MMA-co-HEA) is shown in Figure 3.2. An intense absorbance at 278 nm is characteristic of the vinylene C=C absorbance of the cinnamate group.[13,32,33] The UV absorbance of the precursor poly(MMA-co-HEA) is also shown in Figure 3.2 for comparison. As expected, the unfunctionalized copolymer does not show any distinct absorbance in the UVB region.

### 3.4.2 *In situ* UV irradiation during electrospinning

As mentioned previously, a stable jet was observed to emanate from the apex of the Taylor cone at an electric field strength of 0.75 kV/cm that travels upwards against gravity to the target maintained at ground potential. During its flight to the target, the jet was exposed to the intense unpolarized UV radiation that emanated as a parallel beam from the UV source. The dimensions of the beam emitted from the UV source were ca. 10 cm x 15 cm. The UVB intensity measured at the geometric midpoint of the quartz tube was 13.5 mW/cm$^2$. In an earlier study, Reneker et al. reported the measured jet velocity to be ca. 0.5 m/s.[34] Based on this value, it is estimated that the jet requires ca. 0.2 s to travel through the Quartz tube. Hence, the UV beam should have sufficient intensity to allow adequate irradiation of the cinnamate group in 0.2 s or less. It was found, as will be discussed later, that at an estimated energy exposure of 2.7 mJ/cm$^2$,the cinnamate was able to undergo photodimerization, thereby leading to the formation of intermolecular crosslinks within a given fiber. The aspect ratio of the electrospun jet increases as it undergoes the series of bending electrical instabilities[34] leading to the exposure of a higher surface area to UV irradiation. Because of induced plastic stretching, the polymeric chains in the charged jet are believed to be in a partially extended state.

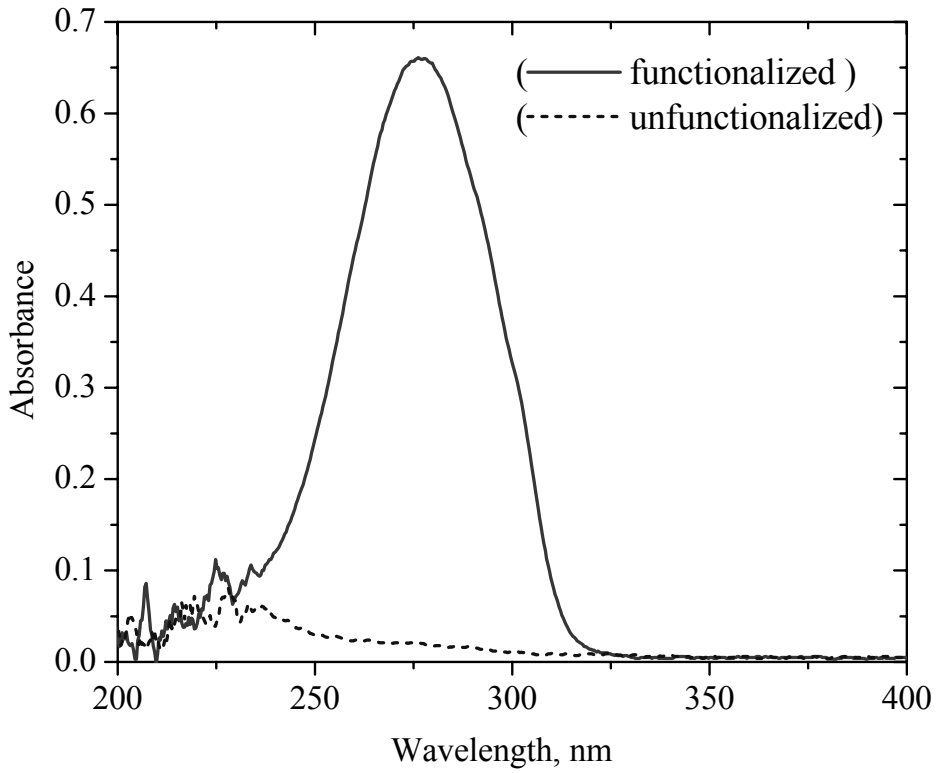


**Figure 3.2** UV absorbance spectra of cinnamate functionalized (4 mol%) poly(MMA-co-HEA) compared to an unfunctionalized poly(MMA-co-HEA)

Therefore the probability of forming intermolecular crosslinks is expected to be more favorable than the formation of intramolecular crosslinks, although the latter cannot be discounted. A low vapor pressure solvent like DMF (b.p. 165 $^{o}$C) does not rapidly evaporate from the jet. As a result, the polymer chains in the jet have sufficient mobility to intermingle and undergo intermolecular crosslinking. In a study involving investigations on formation of inter and intra molecular crosslinks in polymers, Coqueret et al.[35] stated that 'if polymer chains intermingle freely, the likelihood of two adjacent reactant groups belonging to the same chain is small, thereby leading to the formation of mostly intermolecular links.' In addition, intermolecular crosslinks lead to an increase in the molecular weight of the polymer and eventually produce an insoluble gel, whereas intramolecular crosslinks have no such effect. It is noted that the photodimerization of the cinnamate leads to crosslinking of the chains within a single electrospun fiber and not

between the fibers. This was verified by easily pulling out the individual fibers from the irradiated mat by utilizing a pair of tweezers, thereby confirming that the fibers were not attached in the irradiated mat.

The SEM micrographs corresponding to fibrous mats (electrospun with and without UV irradiation) for the three terpolymers are shown in Figure 3.3. As expected, distinct morphological changes were not observed in the electrospun mats after irradiation. Uniform fibers of the functionalized copolymer containing the least amount of cinnamate (4 mol%) had a relatively larger diameter, ca. 2-4 μm in comparison to the fibers of the other two functionalized copolymers that both possessed a diameter of ca. 200-600 nm. This is due to the fact that the zero shear rate viscosity of the solution of functionalized copolymer with 4 mol% cinnamate was larger (2.48 Pa·s) than that of the other two solutions (0.56 and 0.72 Pa·s respectively for solutions of 9 and 13 mol% cinnamate containing copolymers). Some 'beaded' fibers were also observed to form in the case of the functionalized copolymer with the highest amount of cinnamate (13 mol%) (recall Figure 3.3). As reported earlier, the formation of beaded and uniform fibers was related to the polymer solution concentration and viscosity.[28]

**3.4.3 Photochemistry in the electrospun jet**

As mentioned earlier, when cinnamates are exposed to UV, the cinnamate functional group undergoes either photoisomerization or photodimerization (Scheme 3.1). The intramolecular process of photoisomerization is generally favored in dilute solutions[36], at least in the early stages of irradiation.[15-17] The photodimerization of cinnamates arises essentially from head-to-head and head-to-tail [2π+2π] cycloaddition between the double bonds with favorable relative geometry (Scheme 3.2). Due to a brief lifetime of the excited states of benzene derivatives, the two chromophores must be very close to each other to facilitate the dimerization reaction.

The FTIR spectra of poly(MMA-co-HEA) cinnamate electrospun fibers (electrospun with and without UV irradiation) is shown in Figure 3.4. All observed vibrational bands were assigned in accordance with the results reported previously[18,37-42] (Table 3.2). In particular, the band at 1637 $cm^{-1}$ corresponds to the vinylene C=C stretching vibration of the cinnamate group, while the bands at 1388 and 984 $cm^{-1}$

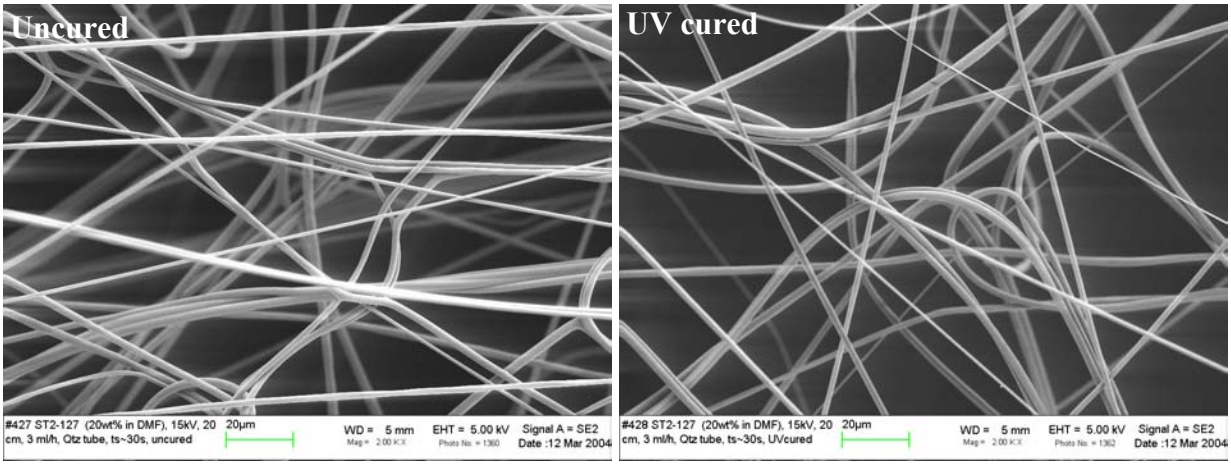


**a)** 4 mol% cinnamate

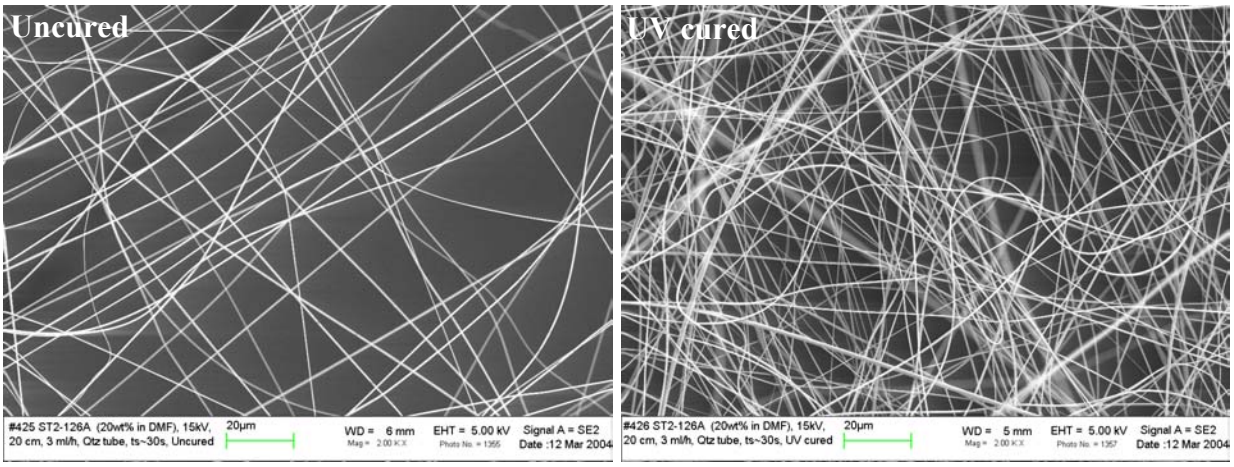


**b)** 9 mol% cinnamate

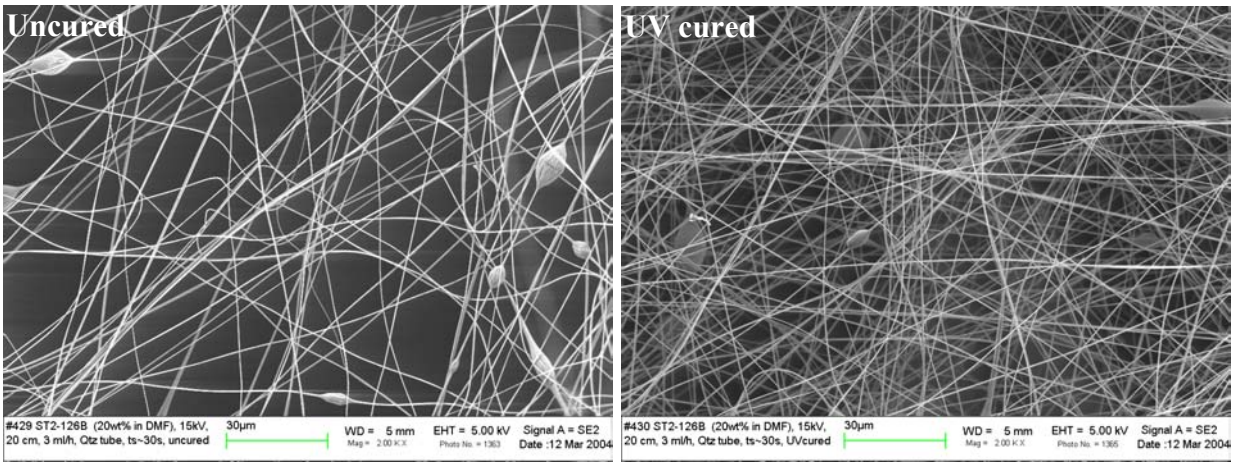


**c)** 13 mol% Cinnamate

**Figure 3.3** SEM micrographs of uncured and UV cured electrospun mats corresponding to a) 4 mol% b) 9 mol% and c) 13 mol% cinnamate. Note that all the micrographs are at same magnification.

**Table 3.2** Characteristic IR bands of poly(MMA-co-HEA) cinnamate

| Wavenumber $cm^{-1}$ | Assignment Description in IR |
|---|---|
| 1637 | C=C stretching vibration of cinnamate |
| 1388 | $C\text{-}CH_3$ bending vibration of atactic PMMA |
| 984 | *trans*-vinylene CH deformation vibration of cinnamate |
| 887 | *cis*-vinylene CH deformation vibration of cinnamate |

correspond to the $C\text{-}CH_3$ bending vibration in MMA and the *trans*- vinylene C-H deformation of this same functional group respectively. A flat baseline was not observed for the spectra reported here. This is due to the fact that the electrospun mats did not have a uniform cross sectional composition (due to its porous nature). As the cross sectional diameter of the detector IR beam was much larger (ca. 100 μm) than the diameter of the fibers (200 nm – 4 μm), it is plausible that certain sections of the beam did not come in contact with solid fibers in the porous electrospun mat. As a result, a non-uniform signal was detected that lead to the non-flat baseline. However, when films cast from the same solutions were analyzed, FTIR peaks were observed to originate from the same minimum values of intensity leading to flat baselines. To compensate for thickness variations in the electrospun samples, the peak intensity at 1388 $cm^{-1}$ corresponding to the bending vibration of the aliphatic $C\text{-}CH_3$ in MMA was used as a reference. This band was selected because the aliphatic $C\text{-}CH_3$ is not involved in the photochemical reactions.

As observed in Figure 3.4, in all three functionalized copolymers, the intensities of the bands at 1637 $cm^{-1}$ and 984 $cm^{-1}$ (due to the vinylene C=C stretching and *trans*-vinylene C-H deformation vibration of the cinnamate groups respectively) decreased with UV irradiation. The intensity drop in the vinylene C=C stretching band results from the conversion of the cinnamate groups due to the photodimerization (Scheme 3.2), while the intensity drop in the *trans*-vinylene C-H deformation vibrational band is distinctly attributed to the consumption of the *trans*-vinylene linkage in the cinnamate group due to *trans-cis* photoisomerization (recall Scheme 3.1) and photodimerization. In order to

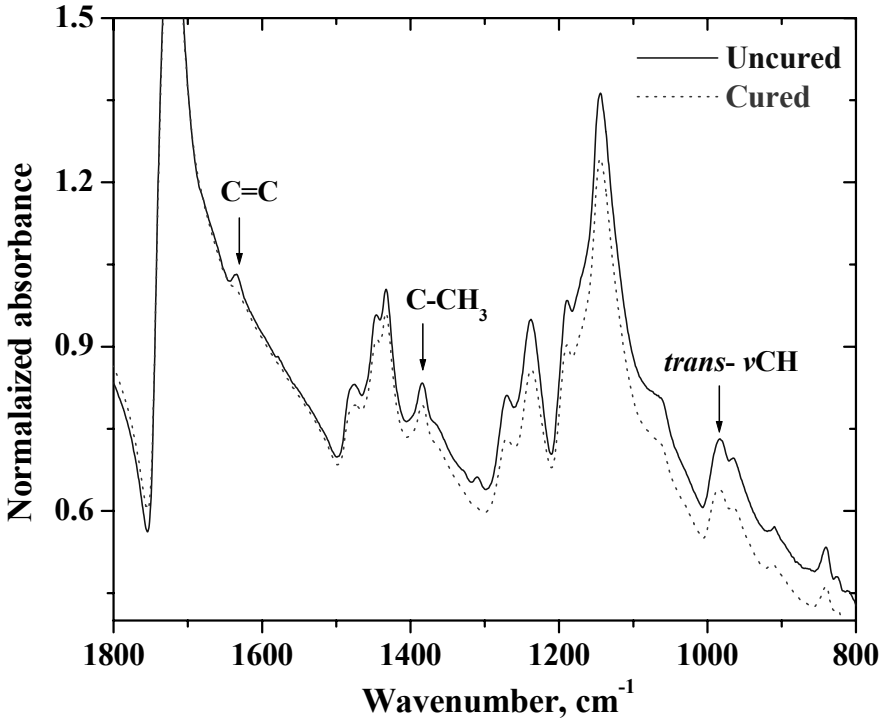


**a)** 4 mol% cinnamate

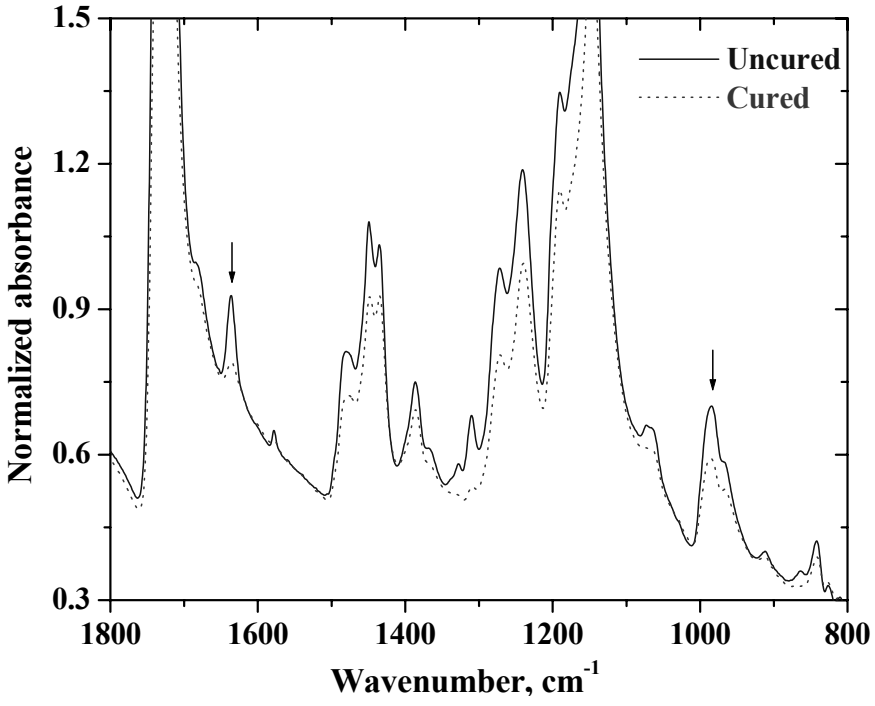


**b)** 9 mol% cinnamate

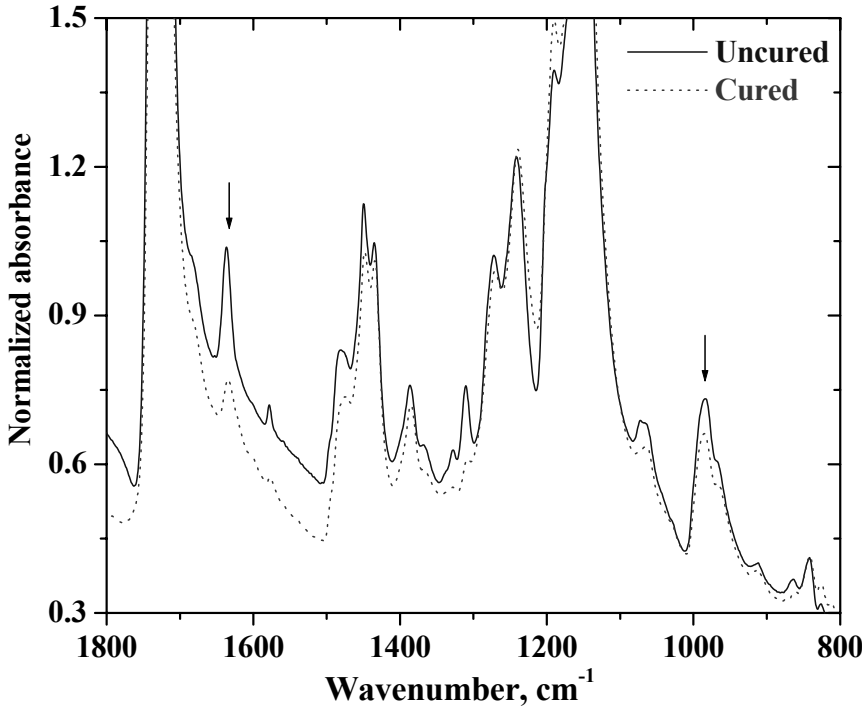


**c)** 13 mol% cinnamate

**Figure 3.4** Absorbance FTIIR spectra of the uncured and UV cured electrospun mats containing a) 4 mol% b) 9 mol% and c) 13 mol% cinnamate.

evaluate the relative reactivity of these two photoreactions, the following relationships are defined:

$$\mathbf{F}_{1637} = 1 - \frac{(\mathbf{I}_{1637} / \mathbf{I}_{1388})_{\mathbf{i}}}{\mathbf{I}_{1637} / \mathbf{I}_{1388})_{\mathbf{o}}} \tag{4.1}$$

$$\mathbf{F}_{984} = 1 - \frac{(\mathbf{I}_{984} /(\mathbf{I}_{1388})_{\mathbf{i}}}{(\mathbf{I}_{984} / \mathbf{I}_{1388})_{\mathbf{o}}} \tag{4.2}$$

where $(\mathbf{I}_{1637} / \mathbf{I}_{1388})_{\mathbf{i}}$ corresponds to the relative intensity of the vinylene C=C bonds *after* irradiation and $(\mathbf{I}_{1637} / \mathbf{I}_{1388})_{\mathbf{o}}$ is the relative intensity of the C=C bonds *before* irradiation. Likewise, in Eq. 4.2, $F_{984}$ quantifies the consumption of trans cinnamate functional groups during *trans-cis* photoisomerization. For the electrospun mats corresponding to the three functionalized copolymers, the values of $F_{1637}$ obtained were 0.008, 0.117 and

0.178 respectively for 4, 9 and 13 mol% of cinnamate incorporated in the copolymer. As expected, the $F_{1637}$ values increase systematically with increasing mol% of the photocurable cinnamate functional group (Figure 3.5). However, at 4 mol% functionalization, only a *very* small fraction (0.8%) of the cinnamate groups undergo photodimerization. Mathematically, this translates to about 0.54 crosslinks per chain in the 4 mol% (calculation based on the number average molecular weight of ca. 170, 000 g/mol)cinnamate functionalized copolymer, indicating the statistical impossibility for the copolymer to form a well developed crosslinked network. At 9 and 13 mol% functionalization, the calculated number of crosslinks per chain are 17 and 39 respectively, which in turn is equivalent to a molecular weight of 10,000 and 4,400 g/mol between crosslinks respectively. The values of $F_{984}$ for the three systems were 0.052, 0.030 and 0.057 respectively for 4, 9 and 13 mol% of cinnamate incorporated in the copolymer. The small positive values of $F_{984}$ indicated that a low level of photoisomerization also took place during the UV irradiation.

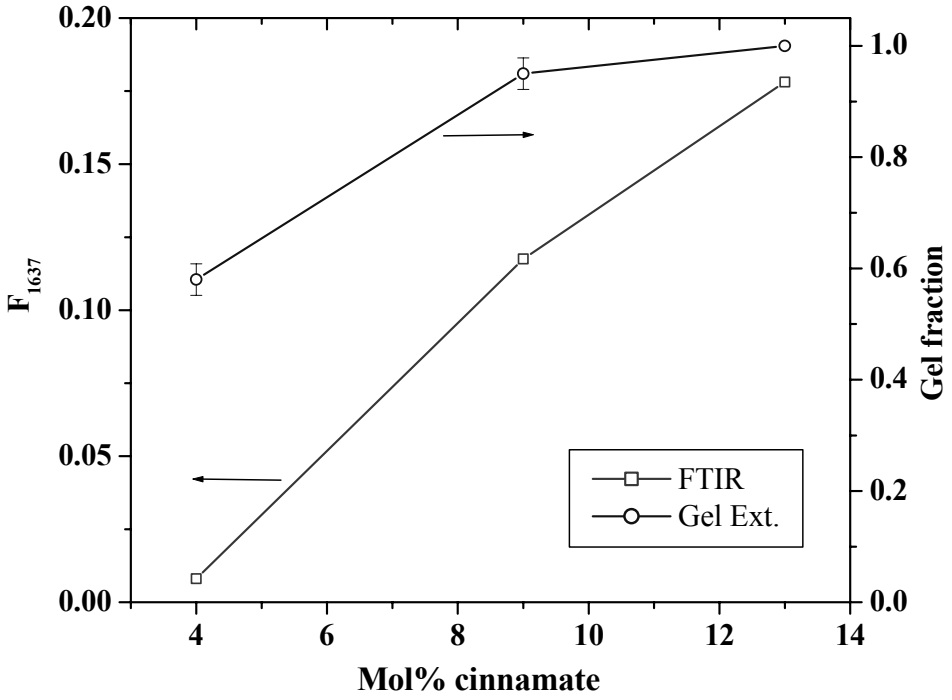


**Figure 3.5** Comparison of the extent of crosslinking as measured by absorbance FTIR and solvent gel extraction.

It is important to note that at 4 mol% functionalization, a higher value of $F_{984}$ than $F_{1637}$ indicates the dominance of photoisomerization over photodimerization. This is attributed to a lesser concentration of cinnamate functional groups. Upon UV irradiation these functional groups undergo photoisomerization instead of photodimerization due to a lack of other cinnamate groups in the immediate vicinity. As the concentration of these functional groups increases, the probability of finding any two spatially close cinnamate groups increases, thereby leading to photodimerization – an observation corroborated by the larger values of $F_{1637}$ than $F_{984}$ at 9 and 13 mol% functionalization respectively.

The irradiated and non-irradiated electrospun mats were also investigated in terms of gel fractions (soxhlet extraction process in refluxing THF for 4 h). The non-irradiated electrospun mats did not exhibit any gel formation (the measured gel fraction was zero for the each of the three systems investigated). For the irradiated electrospun mats, the gel fraction values are plotted in Figure 3.5 (secondary axis). It can be seen that a gel fraction of 58% was attained at 4 mol% cinnamate content. At 9 mol%, nearly 95% gel formation occurred whereas at 13 mol% a 100% gel was observed to form. Recalling the earlier discussion, these results clearly indicated the formation of intermolecular crosslinking due to the photodimerization of the cinnamate functional group. At 9 and 13 mol% of cinnamate content, the irradiated functionalized copolymer formed high levels of gel fraction (95 and 100% respectively), thereby indicating that photodimerization of the cinnamate functional group was the primary photoprocess during UV irradiation.

**3.5 Conclusions**

A *novel* approach to *in situ* crosslinked polymeric fibers that were produced during electrospinning was demonstrated. The *modified* electrospinning apparatus that facilitates *in situ* UV irradiation of electrospun fibers was described. Copolymers of MMA and HEA were synthesized and subsequently functionalized with cinnamoyl chloride. Three functionalized copolymers with different mol% of the cinnamate group (4, 9 and 13 mol% respectively) were utilized in this study. Electrospun fibers of cinnamate functionalized poly(MMA-co-HEA) were successfully crosslinked with UV radiation *while in flight* to the collector target. Subsequent FTIR measurements on UV irradiated and non-irradiated electrospun fibers indicated the [2π+2π] cycloaddition of the

vinylene C=C in addition to the *trans-cis* photoisomerization of the cinnamate species. At 4 mol % functionalization, photoisomerization was the dominant process due to a very low concentration of cinnamate. Further, the irradiated electrospun mats were observed to form a insoluble gel fraction, thereby indicating the formation of intermolecular crosslinks. It was noted that the photodimerization of cinnamate lead to crosslinking between the chains within a single electrospun fiber and not between the fibers.

**Acknowledgements**

This material is based upon work supported by, or in part by, the U.S. Army Research Laboratory and the U.S. Army Research Office under grant number DAAD19-02-1-0275 Macromolecular Architecture for Performance (MAP) MURI. The author thanks Prof. Tim Long and Scott Trenor, Chemistry Department, Virginia Tech for their collaboration and Prof. Chip Frazier, Wood Science Department, Virginia Tech, for allowing the use of AR-1000 Rheometer for viscosity measurements.

**References**

(1) Visconte, L. L. Y.; Andrade, C. T.; Azuma, C. *Journal of Applied Polymer Science* **1998**, *69*, 907-910.

(2) Minsk, L. M.; Smith, J. G.; Deusen, W. P. V.; Wright, J. F. *Journal of Applied Polymer Science* **1959**, *2*, 302-307.

(3) Kvasnikov, E. D.; Kozenkov, V. M.; Barachevsky, V. A. *Zh. Nauchn. Prikl. Fotogr. Kinematogr.* **1979**, *24*, 222.

(4) Barachevsky, V. A. *SPIE* **1991**, *1559*, 184.

(5) Gibbons, W. M.; Shannon, P. J.; Sun, S. T.; Swetlin, B. J. *Nature* **1991**, *351*, 49.

(6) Gibbons, W. M.; Shannon, P. J.; Sun, S. T. *Mol. Cryst. Liq. Cryst.* **1994**, *251*, 191.

(7) Shannon, P. J.; Gibbons, W. M.; Sun, S. T. *Nature* **1994**, *368*, 532.

(8) Iimura, Y.; Kusano, J.; Kobayaashi, S.; Aoyagi, T.; T, S. *Japanese Journal of Applied Physics: Part 2* **1993**, *32*, L93.

(9) Kawanishi, Y.; Tamaki, T.; Sakuragi, M.; Seki, T.; Suzuki, Y.; Ichimura, K. *Langmuir* **1992**, *8*, 2601.

(10) Kawanishi, Y.; Tamaki, T.; Sakuragi, M.; Seki, T.; Ichimura, K. *Mol. Cryst. Liq. Cryst.* **1992**, *218*, 153.

(11) Ichimura, K.; Hayashi, Y.; Akiyama, H.; Ikeda, T.; Ishizuki, N. *Applied Physics Letters* **1993**, *63*, 449.

(12) Robertson, E.; Deusen, W.; Minsk, L. *Journal of Applied Polymer Science* **1959**, *2*, 308-311.

(13) Zheng, Y. J.; Andreopoulos, F. M.; Micic, M.; Huo, Q.; Pham, S. M.; Leblanc, R. M. *Advanced Functional Materials* **2001**, *11*, 37-40.

(14) Kimura, T.; Kim, J.-Y.; Fukuda, T.; Matsuda, H. *Macromolecular Chemistry and Physics* **2002**, *203*, 2344-2350.

(15) Kawatsuki, N.; Matsuyoshi, K.; Hayashi, M.; Takatsuka, H.; Yamamoto, T.; Sangen, O. *Chem. Mater.* **2000**, *12*, 1549.

(16) Rennert, J. J. *Photogr.Sci. Eng.* **1971**, *15*, 60.

(17) Graley, M.; Reiser, A.; Roberts, A. J.; Phillips, D. *Macromolecules* **1981**, *14*, 1752.

(18) Chae, B.; Lee, S. W.; Ree, M.; Jung, Y. M.; Kim, S. B. *Langmuir* **2003**, *19*, 687-695.

(19) Ichimura, K.; Akita, Y.; Akiyama, H.; Kudo, K.; Hayashi, Y. *Macromolecules* **1997**, *30*, 903-911.

(20) Doshi J; Reneker, D. H. *Journal of Electrostatics* **1995**, *35*, 151-160.

(21) Fong, H.; Chun, I.; Reneker, D. H. *Polymer* **1999**, *40*, 4585-4592.

(22) Kim, J.-S.; Reneker, D. H. *Polymer Engineering and Science* **1999**, *39*, 849-854.

(23) Deitzel, J. M.; Kleinmeyer, J. D.; Hirvonen, J. K.; Beck, T. N. C. *Polymer* **2001**, *42*, 8163-8170.

(24) Srinivasan, G.; Reneker, D. H. *Polymer International* **1995**, *36*, 195-201.

(25) Pinto, N. J.; Carrion, P.; Quinones, J. X. *Materials Science and Engineering* **2004**, *A366*, 1-5.

(26) Son, K. S.; Youk, H. J.; Park, W. H. *Biomacromolecules* **2004**, *5*, 197-201.

(27) Zeng, J.; Hou, H.; Wendorff, J. H.; Greiner, A. *Polymer Preprints (American Chemical Society, Division of Polymer Chemistry)* **2003**, *44*, 174-175.

(28) McKee, M. G.; Wilkes, G. L.; Colby, R. H.; Long, T. E. *Macromolecules* **2004**, *37*, 1760-1767.

(29) Yarin, A. L.; Koombhongse, S.; Reneker, D. H. *Journal of Applied Physics* **2001**, *90*, 4836-4846.

(30) Buer, A.; Ugbolue, S. C.; Warner, S. B. *Textile Research Journal* **2001**, *71*, 323-328.

(31) Taylor, G. I. *Proceeedings of the Royal Society, London* **1964**, *280*, 383-397.

(32) Lazarev, V. V.; Barberi, R.; Iovane, M.; Papalino, L.; Blinov, L. M. *Liquid Crystals* **2002**, *29*, 273-279.

(33) Nakayama, Y.; Matsuda, T. *Journal of Polymer Science Part a-Polymer Chemistry* **1992**, *30*, 2451-2457.

(34) Reneker, D. H.; Yarin, A. L.; Fong, H.; Koombhongse, S. *Journal of Applied Physics* **2002**, *87*, 4531-4547.

(35) Reiser, A.; Egerton, P. L. *Macromolecules* **1979**, *12*, 670-673.

(36) Coqueret, X.; El Achari, A.; Hajaiej, A.; Lablache-Combier, A.; Loucheux, C.; Randrianarisoa, L. *Makromol. Chem.* **1991**, *192*, 1517.

(37) Schneider, B.; Stokr, J.; Schmidt, P.; Mihailov, M.; Dirlikov, S.; Peeva, N. *Polymer* **1979**, *20*, 705-712.

(38) Dybal, J.; Krimm, S. *Macromolecules* **1990**, *23*, 1301-1308.

(39) Perny, S.; Le Barny, P.; Delaire, J.; Buffeteau, T.; Sourisseau, C. *Liquid Crystals* **2000**, *27*, 341-348.

(40) Perny, S.; Le Barny, P.; Delaire, J.; Buffeteau, T.; Sourisseau, C.; Dozov, I.; Forget, S.; Martinot-Lagarde, P. *Liquid Crystals* **2000**, *27*, 329-340.

(41) Perny, S.; Le Barny, P.; Delaire, J.; Dozov, I.; Forget, S.; Auroy, P. *Liquid Crystals* **2000**, *27*, 349-358.

(42) Oriol, L.; Pinol, M.; Serrano, J. L.; Tejedor, R. M. *Journal of Photochemistry and Photobiology a-Chemistry* **2003**, *155*, 37-45.